Electrochimica Acta 318 (2019) 504–512

Contents lists available at ScienceDirect

Electrochimica Acta

journal homepage: www.elsevier.com/locate/electacta

Stress-charge coupling coefficient for thin-film polypyrrole actuators – Investigation of capacitive ion exchange in the oxidized state

Benedikt Roschning [a, *], Jörg Weissmüller [a, b]

[a] Institute of Materials Physics and Technology, Hamburg University of Technology, Hamburg, Germany
[b] Institute of Materials Research, Materials Mechanics, Helmholtz-Zentrum Geesthacht, Geesthacht, Germany

ARTICLE INFO

Article history:
Received 9 April 2019
Received in revised form
15 May 2019
Accepted 31 May 2019
Available online 3 June 2019

Keywords:
Polypyrrole
Actuation
Stress-charge coupling
Strain-charge coupling
Plane stress

ABSTRACT

This work quantifies the actuation behavior of thin electrodeposited polypyrrole films on rigid substrates. During in situ cantilever bending experiments in aqueous perchloric acid, the films remain clamped to their substrate and the film stress is inferred from a small bending of the cantilever. The potential range under study is 0.4–0.8 V versus the standard hydrogen electrode. Within this potential region, the film is in the oxidized state and the actuation arises from capacitive electrode processes. For the volumetric capacitance, c^*, we find 0.24 ± 0.01 F/mm^3. The stress-charge coupling coefficient, ξ, which is defined as the stress variation per volumetric charge density, emerges as − 153 ± 11 mV. The results are robust, reproducible and independent of the film thickness or the potential scan rate. The experimental value of ξ is supported by an independent estimate, based on a micromechanical model in combination with literature data for the partial molar volume of solvated perchlorate anions and the elastic constants of polypyrrole.

1. Introduction

Since the discovery of electrically conductive polymers in the 1970s [1–3], polypyrrole (PPy) has attracted great attention because of its high electrical conductivity and good environmental stability [4]. An electrochemically induced change in oxidation state creates delocalized charge carriers along the polymer backbone [5]. To ensure charge neutrality, ions are exchanged between the permeable polymer and the surrounding electrolyte [5]. The change in oxidation state influences the electrical conductivity [1,2], the optical absorption [6], the ionic permeability [7,8] and the mechanical properties [9,10]. This opens up pathways for the development of electro-chemical sensors [11,12], transistors [13], smart membranes [14], capacitors [15,16] and batteries [17]. The polymer swells as it absorbs solvated ions [18]. This property, along with electrochemical cycling stability [19], a low operating voltage [20] and strains up to 40% [19,21–23] make PPy an interesting material for actuation [18,24–27].

The change, δ, in strain, ε, of unsupported, stress-free PPy films is proportional to the change in charge density, q_V (charge per volume) [9,18,25,26,28–30]. This finding is consistent with the well-established notion that the microscopic process behind the swelling is the incorporation of ions [5,18,25,30–34]. Reported values for the uniaxial strain-charge coupling coefficient, $\psi = \delta\varepsilon/\delta q_V$, cover a remarkably wide range, between 0.03 and 0.5 mm^3 /C, depending on the nature of the ion, the solvent and the synthesis conditions [5,29,30,35,36].

PPy is typically restricted to thin film geometries with thicknesses not exceeding a few micron. Macroscopic actuators therefore require a supporting substrate, to which the film remains clamped. Proposed architectures are bilayered bending cantilevers [37,38], multilayered axial strain actuators [14] or coated fibers spun to yarns [26]. Another approach, in which actuators can be operated in air, is the arrangement of a solid polymer electrolyte between two layers of conducting polymer [39–42]. In all these scenarios the actuation may be understood as the consequence of stresses in the clamped PPy film acting on a substrate rather than a direct, free straining of the PPy. Because q_V parameterizes the ion uptake which prompts the actuation, a quantitative prediction of the performance of PPy-based actuators requires numerical values for the generated stress, σ, per charge density. In other words, the stress-charge coupling coefficient, defined as $\xi = \delta\sigma/\delta q_V$, represents a fundamental quantity in this context. The purpose of the present work is the investigation of the magnitude of ξ for clamped

* Corresponding author.
E-mail address: benedikt.roschning@tuhh.de (B. Roschning).

https://doi.org/10.1016/j.electacta.2019.05.166

PPy films.

By its definition, ξ is similar to the electrocapillary coupling parameter [43], which quantifies the surface stress response of metals to changes in their superficial charge density. This parameter has been explored by experiment and ab initio simulation [44–47]. Ab initio simulation shows that changes in surface stress arise, because a polarization of the interface changes the electron density within the bonding regions between the atoms and within the screening orbitals around their cores [47]. Both changes modify the bond strength [47].

It is well acknowledged that the film stress in PPy is proportional to the transferred charge. However, the few studies [48,49] investigating the stress-charge relation do not report the volumetric charge density and so fall short of measuring ξ. One may argue that ξ may be estimated from the strain-charge coupling and the elastic properties of the film, yet this approach has not been pursued. In fact, this strategy is compromised by the strong dependency of the elastic properties of PPy on the manufacturing conditions, on the oxidation state and changes with increasing external load [9,10].

Recent PPy-based actuator architectures propose the use of stiff skeleton structures as substrates, specifically multi-walled carbon nanotube networks [50,51], electrospun microribbons [52] and open-porous metal nanoskeletons [53]. Coating the backbone structure with a nm-thick PPy layer enables the combination of active PPy films with a mm-sized, 3D actuator geometry. In comparison to μm-thick PPy films, where the response rate is slow due to the sluggish ion diffusion in and out of the PPy network [20,40,54], the nanoskeletons with their nm-sized coating allow a fast ion transport to and through the polymer. This new approach enables fast actuation in mm-sized geometries. In this context it is of interest whether the coupling becomes thickness-dependent in the limit of decreasing film height. This question arises, because—as mentioned above—clean metal surfaces (without PPy) exhibit a strong surface-stress charge coupling [44,45,47,55,56], which results in significant actuation as well [57–59]. In other words, the effective stress-charge coupling of PPy-coated metal surfaces cannot extrapolate to zero in the limit of vanishing film thickness.

In this work, we present an experimental study on the stress-charge coupling of $\sim 10-100$ nm thin PPy films in aqueous perchloric acid. We study stiff silicon cantilevers, coated on one side with PPy. The film was operated as capacitor in the oxidized regime within the potential window of 0.4–0.8 V versus the standard hydrogen electrode. During cyclic voltammetry, a slight change in curvature of the cantilever allows us to precisely quantify the stress evolution. The transferred charge is recorded simultaneously. The resulting stress-charge coupling is compared to an independent estimate based on a micromechanical analysis of the stress in a clamped film, along with literature data for the relevant materials parameters.

2. Methods

Our specimens were multilayered beam structures. Double side polished (100)-oriented silicon wafers of 100 μm thickness with a 100 nm thick thermally grown oxide layer (Si-Mat Silicon Materials) were cut into rectangles of 8×40 mm^2 with the edges along the $<110>$ directions. They were coated on one side with 40 nm of gold by DC magnetron sputtering, using a 2 nm titanium adhesion layer. For stress relief, the samples were annealed at 300° C for 1 h in a vacuum of 10^{-6} mbar. The procedures and equipment were the same as in Refs. [44,46], where further details, such as the surface roughness and the texture, can be found. The substrates represent electrically isolated (by the oxide layer) silicon with a thin conductive gold layer on top. This gold layer serves as working electrode during the PPy deposition and as electrical contact. Its geometry defines the electrochemically active surface area, thus the footprint of the PPy film. For each individual specimen, this area was measured to an accuracy $< 1\%$ using a calibrated microscope.

PPy was electropolymerized according to Ref. [60] in a solution of 0.1 M pyrrole and 0.1 M lithium perchlorate ($LiClO_4$) in acetonitrile and 2% ultrapure water (18.2 MΩ cm) at a constant potential of 900 mV vs. an Ag/AgCl (in 3M KCl) reference electrode. Before deposition, the pyrrole was distilled at 130° C and ambient pressure. A platinum mesh, placed parallel to the working electrode, was used as counter electrode. The thickness of the deposited PPy films, h_f, was determined from the transferred superficial charge density, Δq, according to Refs. [61,62].

$$h_f = 2.5\ \text{nm} \Big/ \left(\text{mC} \Big/ \text{cm}^2\right) \Delta q \tag{1}$$

Atomic force microscopy (AFM, JPK NanoWizard 4 in QI mode, which is a force-resolved quantitative imaging contact mode) was used to verify the empirical charge-thickness relation. After a part of the PPy film was removed from the substrate by adhesive tape, AFM images were taken at the resulting edge to detect its height.

All electrochemical characterizations were performed in 1 M perchloric acid ($HClO_4$), prepared from $HClO_4$ (Suprapure, Merck) and ultrapure water (18.2 MΩ cm), deareated with argon. A reversible hydrogen electrode (Gaskatel HydroFlex) served as reference electrode and all potentials are specified versus the standard hydrogen electrode (SHE). The capacitive charging was characterized by a potentiostat (Metrohm Autolab PGSTAT 302N). A linear scan generator allowed a continuous current measurement, which is necessary for precise integration of the transferred electric charge. At low nominal potential scan rates, the linear scan generator produced slightly asymmetric scans. As a typical example, a nominal scan rate of 10 mV/s implied true anodic and cathodic scan rates of 8.6 and 11.4 mV/s, respectively. This did not impair the data for capacitance or charge, because the capacitance was averaged over both scan directions and the charge was determined by integration of current over time.

The variation in substrate curvature during potential cycling was determined by a multiple-beam laser setup (kSA MOS) equipped with a CCD camera; see details in Refs. [44,46,63–65]. For maximal resolution, the complete measuring arrangement was mounted on a vibration isolated table and the room was air conditioned at 21° C. With these actions, vibrational effects of air flow or impact noise as well as thermal drift were minimized.

A sketch of the experimental setup is shown in Fig. 1. The electrochemical cell was made of polytetrafluoroethylene (PTFE) and sealed with a 2 mm thick slide of borsilicate glass and a viton o-ring. The cantilever was mounted with the polished silicon backside facing the laser, ensuring a good reflectivity independent of the PPy film thickness. A gold plate with a surface area of 5 cm^2 was used as counter electrode. Both electrodes as well as the reference electrode were immersed in electrolyte and connected to a potentiostat. A 3×3 array of parallel laser beams was projected onto the silicon wafer. The incidence was normal (incident angle $\alpha = 0°$) in the plane depicted in Fig. 1; this is also the plane in which the curvature change was measured. Separation of incident and reflected beams was achieved by tilting the incident beams by $\beta = 3°$ away from the normal, in the out-of-plane direction of Fig. 1. The reflected beams were detected by the CCD at the distance, $L = 110.0$ cm, from the substrate. The spot spacing in the (arbitrary) reference state is d_0. If the wafer bends up or down, the spacing, d, varies, and the change in curvature, $\Delta\kappa$, is calculated from this variation according to [44,46,64]

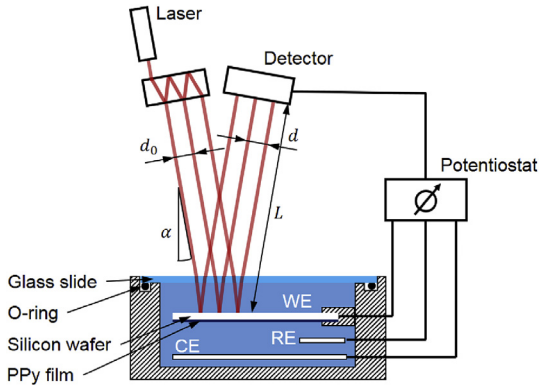

Fig. 1. Experimental setup for in situ films stress measurements. The electrochemical cell is made of polytetrafluoroethylene (PTFE) and sealed with an optical transparent glass slide and a viton o-ring. The cantilever working electrode (WE), made from silicon with a polypyrrole film on top, the reversible hydrogen reference electrode (RE) and the gold counter electrode (CE) are immersed in electrolyte. The electrodes are connected to a potentiostat in a three-electrode set up. The array of laser beams passes the glass slide and electrolyte, gets reflected on the backside of the wafer and hits the detector. L denotes the distance wafer-detector, α the angle between the incident laser beams and the normal to the surface and d the distance between the individual laser beams.

$$\Delta\kappa = \frac{\cos\alpha}{2Ln}\,\frac{d-d_0}{d_0} \tag{2}$$

with n the refractive index of the electrolyte. In the case of diluted electrolytes n takes the value of pure water, $n = 1.33$ [44,64]. The cell window was thin enough to neglect the refraction at the air/glass and glass/liquid interfaces [44,64]. As demonstrated in the results section, the resolution of our setup is $\Delta\kappa = 4\times\ 10^{-6}\ \mathrm{m}^{-1}$. In other words, curvature changes with a radius as large as 250 km can be reliably detected.

Assuming the film stress, σ, to be isotropic in the substrate plane, the Stoney equation [66,67] relates σ to $\Delta\kappa$ by

$$\Delta\sigma = \frac{M_S}{6}\,\frac{h_S^2}{h_f}\,\Delta\kappa \tag{3}$$

M_S and h_S denote the biaxial modulus and height of the substrate, respectively. Because of its orthotropic elasticity and symmetry in the (1 0 0) crystal plane, the biaxial modulus of our silicon substrates can be treated by a single value, $M_S = C_{11} + C_{12} - \frac{2C_{12}^2}{C_{11}} =$ 181 GPa, with C_{ij} the single-crystal stiffness parameters [68].

It is noteworthy that the evaluation of the film stress based on eq (3) requires only knowledge of the elastic parameters of the substrate. The elastic response of the film does not enter. This reflects the fact that the bending stiffness of the cantilever is dominated by the thick and stiff silicon substrate. In fact, our cantilevers are well within the condition for ignoring the film contribution to the bending stiffness, namely $h_f/h_s < 2\times10^{-3}$ [67]. An in-depth discussion showing that the elastic properties of the film are indeed negligible can be found in the Supporting Information. In the experiment, the substrate acts as measurement device.

3. Results

3.1. Deposition and film thickness

Fig. 2 shows the current density, j, and the change in charge density, Δq, versus time, t, at a constant deposition potential of 900 mV vs. Ag/AgCl (3M KCl). The current density (left ordinate)

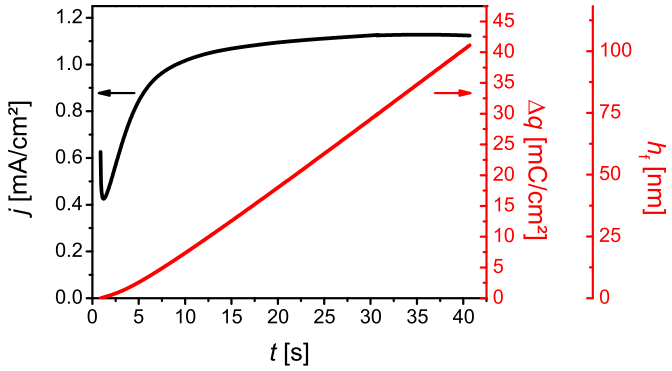

Fig. 2. Kinetics of electrodeposition. Current density, j, (black graph and left ordinate) and charge density, Δq, (red graph and right ordinate) versus time, t, at a constant deposition potential of 900 mV relative to a silver/silverchloride reference electrode. The film thickness, h_f, (second right ordinate) was calculated using eq (1). Data is for the example of the thickest film under study.

passes a minimum during the first seconds and then approaches a steady value of $\sim 1.1\ \mathrm{mA/cm^2}$. The current minimum can be related to a nucleation-conformational relaxation and chemical kinetic control [60]. After a short break-in period, the transferred charge (right ordinate) increases linearly with time. This is consistent with a diffusion-controlled deposition [60]. The estimated film thickness, based on eq (1), is shown as the additional right ordinate. The film thickness can be tuned by the deposition time.

Fig. 3a depicts an AFM image at the edge of a PPy film. The film (on the left-hand side) appears to be dense and of uniform thickness. A height profile is shown in Fig. 3b. The step height suggests $h_f = 106 \pm 6$ nm. This is in excellent agreement with the value, 103 nm, which is estimated from the transferred charge using eq (1). The AFM- and charge-based thickness values of all specimens in

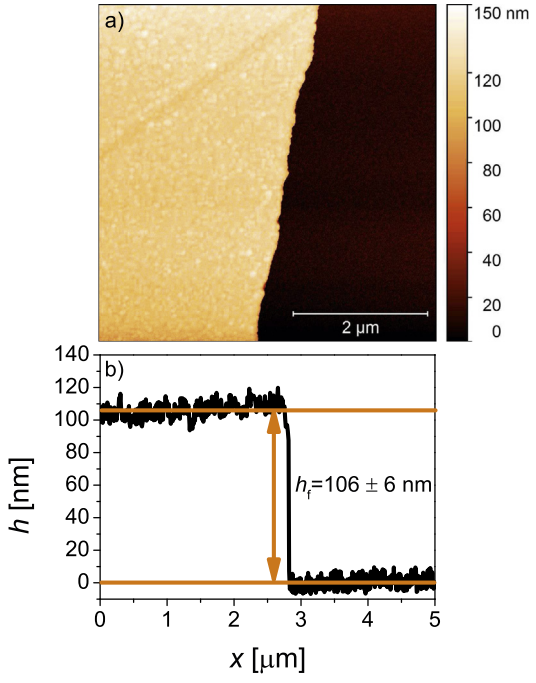

Fig. 3. Measuring the film thickness. a) Atomic force microscopy image of the region near the edge of the polypyrrole film. b) Height profile across the film edge, in the center of the image in a). Data is for the example of the thickest film under study.

our study are shown in Table 1. The table provides further support for the validity of eq (1).

3.2. Electrochemical characterization

Prior to characterizing the electrochemical and the actuation behavior, each of our specimens was subjected to at least 20 blind potential cycles in the same potential interval as the actual measurement. It was found that samples conditioned this way provided stationary, reproducible electrochemical and actuation behavior over at least 10 repetitions. As an example, Fig. 4 shows the volumetric current density, j_V, and the volumetric charge variation, Δq_V, over time for the thinnest film (9 nm) under study. The nominal scan rate was 10 mV/s and the vertex potentials were 0.4 and 0.8 V versus SHE. It can be seen that the transferred charge is perfectly recoverable.

Based on the electrode area and the thickness of the PPy film we converted the experimental current densities to volumetric values, j_V. Fig. 5a shows exemplary cyclic voltammograms (CVs) of j_V versus the electrode potential, E, for one of our films. The potential range of our study was 0.4–0.8 V with sweep rates, $\dot{E}$, from 10 to 50 mV/s. The rectangular appearance of the CVs suggests capacitive or pseudo-capacitive behavior. This observation is consistent with previous observations [29] which locate the present potential range in the oxidized regime of the PPy.

Our potential range is motivated as follows: Studies on the overoxidation of PPy showed degradation above potentials of 0.9 V vs. SHE [69]. To obtain a stable electrochemical behavior over repeated cycles, we chose the upper vertex potential as 0.8 V, below the aforementioned degradation potential. At this potential, the PPy is in the oxidized state with delocalized positive charges along its backbone [4]. To remove these charges, thus to reduce the PPy, more negative potentials, below 0 V vs. SHE, would be necessary [70]. In our experiments, a noticeable faradaic current was observed for potentials below 0.4 V. This current is undesired, because it would impair the precise determination of the charge which is recoverably stored in the PPy film. The faradaic current in our experiment may tentatively be attributed to the oxygen reduction reaction [71] and is characteristic for the use of an aqueous electrolyte. The faradaic current could be suppressed by in situ sparging. However, this approach is incompatible with our cantilever bending experiment, because sparging would induce vibrations which interfere with the curvature measurement. Therefore, we restricted the lower vertex potential to 0.4 V.

Fig. 5b depicts the mean magnitude of j_V versus $\dot{E}$ for all specimens under study. It is seen that j_V increases linearly with $\dot{E}$, confirming that the PPy electrode behaves like a capacitor. The linearity is consistently found for all films, independent of their thickness. We conclude that all potential scan rates in our experiment are sufficiently slow for the charge to equilibrate at each potential. In other words, the transferred charge in our experiments reflects the capacity at equilibrium and is not affected by transport limitations. The slope of j_V versus $\dot{E}$ then represents the differential volumetric capacitance, which may be defined as

$$c^* = \delta q_V / \delta E \tag{4}$$

Linear regression yields $c^* = 0.24 \pm 0.01$ F/mm^3, with the standard error as uncertainty. This capacitance value is substantially larger than the previously reported value of 0.13 F/mm^3 for PPy doped with a different anion, hexafluorophosphate [29].

Table 1
Characterization of the films under study. Charge density, Δq, transferred during electropolymerization and film thickness, h_f, as estimated from the deposition charge and eq (1) (subscript 'charge') or measured by atomic force microscopy (subscript 'AFM').

Δq [mC/cm^2]	$h_{f,charge}$ [nm]	$h_{f,AFM}$ [nm]
3.6	9	–
7.8	20	–
16.2	40	–
28.3	71	63±6
30.0	75	–
41.3	103	106±6

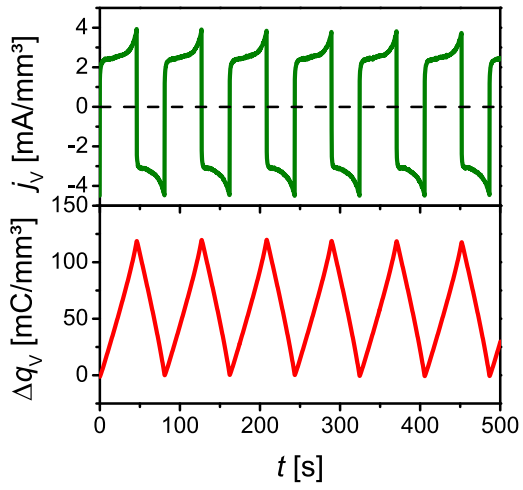

Fig. 4. Reproducibility of electrochemical behavior. Current, j_V (top), and charge variation, Δq_V (bottom), over time, t, for the thinnest film (9 nm thickness) under study. Scan rate 10 mV/s, vertex potentials 0.4 and 0.8 V versus SHE.

3.3. In situ curvature measurements

Fig. 6 exemplifies the data analysis for the in situ substrate bending experiment. Parts a) and b) show the potential variation over time and the simultaneous variation in differential spot spacing, $(d - d_0)/d_0$, respectively. It is seen that the differential spot spacing varies in phase with the potential, with a highly reproducible amplitude and with no apparent noise on the scale of the figure. This finding suggests that the actuation behavior of the polypyrrole film is stable during subsequent potential cycles and that the stress evolution, which underlies the spot spacing, is excellently resolved by our setup.

Fig. 6c depicts the curvature variation, $\Delta\kappa$, which is inferred from the differential spot spacing based on eq (2). The red graph in Fig. 6c represents a straight line of best fit in a linear section of the experimental $\Delta\kappa(t)$ graph. Fig. 6d plots the difference between $\Delta\kappa(t)$ and the fit. The standard deviation, 4×10^{-6} m^{-1}, is illustrated by the shaded area in the figure. This quantity provides an estimate for the resolution of our experimental setup. The resolution in curvature translates into a resolution of 250 km in bending radius. This is superior, by roughly the factor of 5, compared to early implementations of the same approach [63]. It can be seen in Fig. 6c that the peak-to-peak amplitude of $\Delta\kappa$ for our thinnest film under study is 6×10^{-4} m^{-1}. This value is more than two orders of magnitude larger than the resolution, emphasizing that our setup is more than sufficient to determine the in situ curvature changes. Note that the data of Fig. 6 refers to the thinnest among our films, $h = 9$ nm; all other films provided even stronger bending amplitude.

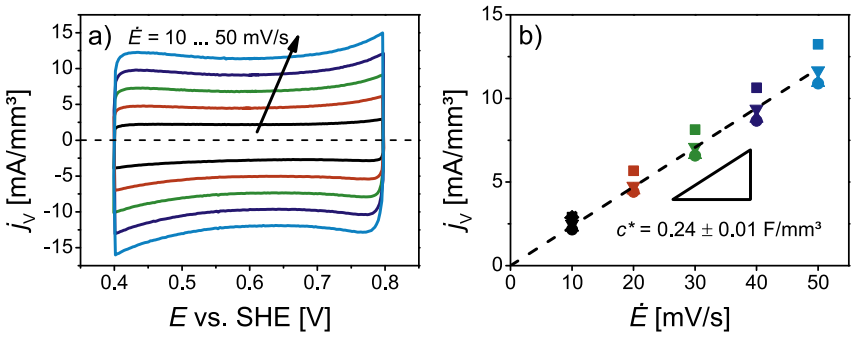

Fig. 5. Characterizing the capacitance. a) Exemplary cyclic voltammograms of the volumetric current density, j_V, versus the electrode potential, E, measured relative to the standard hydrogen electrode (SHE). Sweep rates, $\dot{E}$, vary from 10 mV/s to 50 mV/s in steps of 10 mV/s. b) Mean values of j_V versus $\dot{E}$. Dashed line: Linear regression with the slope corresponding to the volumetric capacitance, c^*. Different symbols denote the individual specimens used in this study. Some symbols overlap.

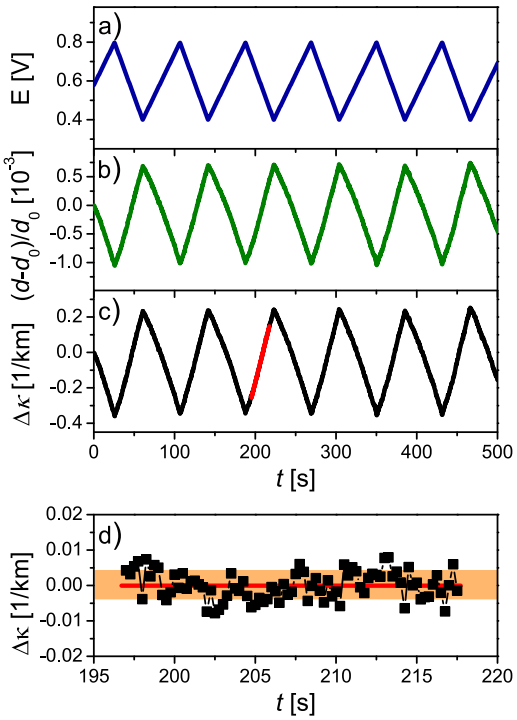

Fig. 6. Resolution of the in situ substrate bending study. Electrochemical and mechanical data recorded simultaneously during six successive potential cycles for the thinnest film (9 nm thickness) under study. a) Electrode potential, E, versus time, t. b) Differential spot spacing, $(d - d_0)/d_0$, versus t. c) Curvature, $\Delta\kappa$, over t. Red line: Straight line of best fit in a linear section of the $\Delta\kappa(t)$ graph. d) Difference between experimental curvature change and fit of subfigure c). Mean square deviation between data and fit (illustrated by shaded region) indicates resolution in curvature.

3.4. Stress-charge coupling

Fig. 7 exemplifies results of an in situ actuation experiment based on potential cycles at the nominal scan rate of 10 mV/s, for the thinnest film of our study (h = 9 nm). The top part of the figure shows the electrochemical characterization. The cyclic voltammogram in subfigure a) is consistent with Fig. 5a. Fig. 7b shows that the volumetric charge density depends linearly on the potential. There is little hysteresis. The charge graph is perfectly closed, suggesting a nearly ideal capacitive process with no noticeable faradaic side reactions.

We now turn to the characterization of the film stress. Recall that the stress variation, $\Delta\sigma$, is obtained from curvature data as in Fig. 6c by means of eq (3). The two graphs in the bottom half of Fig. 7 show the results. Fig. 7c depicts $\Delta\sigma$ versus E during potential cycling. Similar to the change in charge density, the change of the film stress over the potential is almost free of hysteresis. The graph is closed, suggesting no noticeable drift and, hence, a good film adhesion to the substrate. It can be seen, that $\Delta\sigma$ is approximately linear to E, notably at the lower potential values. Fig. 7d shows a plot of $\Delta\sigma$ versus Δq_V. This representation provides a highly linear graph, specifically in the region corresponding to $E < 0.7$ V vs. SHE. Furthermore, the small hysteresis which is observed in the charge-potential and the stress-potential graphs is completely removed. This observation suggests that the film stress is inherently governed by the charge density, as opposed to the potential. The linearity and the lack of hysteresis in $\Delta\sigma(q_V)$ support the stress-charge coupling coefficient, ξ, as a key materials parameter quantifying the electro-chemo-mechanical coupling behind the actuation of PPy.

The magnitude of ξ is obtained by fitting the linear section of graphs such as Fig. 7d. Note that, as a consequence of its definition, ξ has the unit volts. Our results for ξ, based on experiments with films of thicknesses between 9 and 103 nm, are summarized in Fig. 8. The figure illustrates the excellent reproducibility of the coupling coefficient. Furthermore, the results indicate that the coupling strength is independent of the film thickness within the entire interval of our study. If we accept the notion of a constant value for the coupling coefficient, averaging over the data suggest $\xi = -153 \pm 11$ mV, with the standard deviation as error.

In an additional experiment the potential was stepped from 0.4 to 0.8 V and held constant, while the evolution of the film stress was tracked over time. After no further change in film stress was detected, the potential was stepped back to 0.4 V and the stress evolution was tracked again. For all specimens under study the film stress immediately reached a constant value, suggesting that ion exchange is faster than the acquisition rate of our cantilever bending setup, ~200 ms (see Figure S1 of the Supporting Information).

4. Discussion and conclusions

Our study is based on in situ stress variation measurements during potential cycling, using a series of PPy films with thicknesses between 9 and 103 nm. As quantifiable parameters we measure the volumetric capacitance, c^*, and the stress-charge coupling coefficient, ξ. For both parameters we find a high reproducibility and no dependency on the film thickness or the potential sweep rate. This appears to qualify our values, $c^* = 0.24 \pm 0.01$ F/mm³ and $\xi = -153 \pm 11$ mV, as robust and reliable. The lack of a sweep-rate

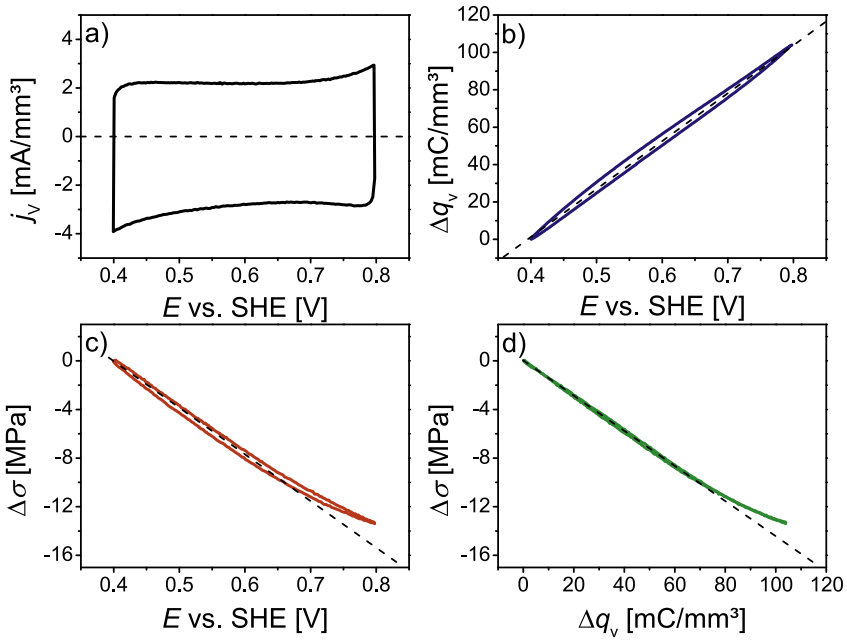

Fig. 7. Characterizing the electrochemical actuation behavior. In situ substrate bending study for the thinnest film (9 nm thickness) under study. Potential sweep rate 10 mV /s. a) Volumetric current density, j_V, versus applied potential, E. b) Transferred volumetric charge density, Δq_V, versus E. c) Change in film stress, $\Delta\sigma$, versus E. d) $\Delta\sigma$ versus Δq_V. Dashed lines in b) and c) illustrate linear behavior. Dashed line in d): Straight line of best fit in the linear region of the graph. The slope of this line provides the stress-charge coupling coefficient, ξ.

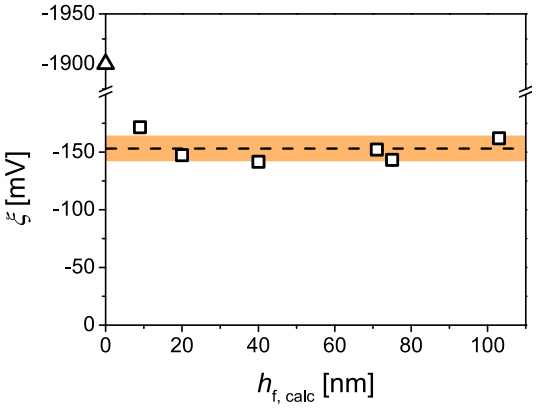

Fig. 8. Stress-charge coupling. Stress-charge coupling coefficient, ξ, versus film thickness $h_{f,calc}$. Mean value and standard deviation in ξ are shown as the dashed line and the shaded area, respectively. Symbol at $h_{f,calc} = 0$ (△) refers to the electrocapillary coupling parameter of the clean gold surface; note axis break in the ordinate.

dependence, along with the findings from our potential step experiments, imply that the charging time of our films is in the order of a few hundred milliseconds or below. This finding is in good agreement to previous experimental results [72], where it was shown that equilibration of 1 μm thick PPy films takes up to 2 s. Therefore, the determined parameters represent the equilibrium behavior of PPy during electrochemical charging and actuation.

Due to the limited potential range, our experiments were performed in the oxidized state and the films were operated as supercapacitors. During a positive-going potential scan, electrons will be withdrawn from the polymer chains and anions incorporated for electric compensation. This process is charge recoverable, in other words, nonfaradic [73]. For a phenomenological description it is irrelevant whether or not new chemical bonds are formed along with the exchange of anions. The essential quantities are simply the transferred recoverable charge and the mechanical response.

Substantial surface stress is generated when clean (no PPy) metal electrode surfaces are polarized. At $\xi = -1.9$ V [44,45,74], the associated coupling parameter is more than ten times larger than that of PPy. A data point at $h_f = 0$ in Fig. 8 illustrates the clean metal surface behavior. The electro-chemo-mechanical coupling of the clean surface may be expected to dominate the stress-charge signature in the limit of vanishing film thickness. It is therefore significant that our experiments find the value of ξ constant, down to the thinnest (9 nm) film under study. We conclude that the electrode potential drop is screened within the PPy film. In other words, a variation of the electrode potential does not affect the space charge region at the metal-PPy interface. The coupling signature of the metal will only be observable for even thinner PPy films.

We now discuss the micromechanical response of the in-plane film stress and of the out-of-plane strain to charge transfer. Because the substrate is thick and rigid in comparison to the PPy film, the in-plane film strain is negligible in an analysis of the stress-charge relation during ion exchange. The following thought experiment explores the stress in the clamped film. In a first step, consider the PPy film detached from the substrate and then charged while free of stress. This will lead to an isotropic strain and to the relative volume change

$$\delta\varepsilon = -\frac{\Omega}{zF}\delta q_V \tag{5}$$

with z, Ω and F the signed ionic valency, the molar volume of the exchanged ion and the Faraday constant, respectively. In a second step, an isotropic in-plane strain of the magnitude $-\delta\varepsilon/3$ brings the film back into registry with the substrate. The plane stress developed during this step is the film stress, σ. Accounting for eq (5) and for Hooke's law, along with the boundary condition of free expansion normal to the substrate surface, the variation of σ is

found as

$$\delta\sigma = \frac{Y}{3(1-\nu)}\frac{\Omega}{zF}\delta q_V \tag{6}$$

where Y is Young's modulus and ν Poisson's ratio. The out-of-plane strain, $\delta\varepsilon_z$, is the sum of two contributions. Firstly, $\delta\varepsilon/3$ is the free expansion in normal direction during step 1. Secondly, $-2\nu\delta\sigma/Y$ is the transverse elastic straining during step 2, which follows from Hooke's law. Accounting for eq (6), one thus finds

$$\delta\varepsilon_z = -\frac{1+\nu}{3(1-\nu)}\frac{\Omega}{zF}\delta q_V \tag{7}$$

Equations (5)–(7) express the charge-related coupling parameters for the linear strain of free-standing PPy films, ψ, the out-of-plane strain of clamped films, ψ_z, and the in-plane stress, ξ, respectively. Rearranging yields

$$\psi = \frac{1}{3}\frac{\delta\varepsilon}{\delta q_V} = -\frac{1}{3}\frac{\Omega}{zF} \tag{8}$$

$$\psi_z = \frac{\delta\varepsilon_z}{\delta q_V} = -\frac{1+\nu}{3(1-\nu)}\frac{\Omega}{zF} \tag{9}$$

$$\xi = \frac{\delta\sigma}{\delta q_V} = \frac{Y}{3(1-\nu)}\frac{\Omega}{zF} \tag{10}$$

The above equations result directly from the mechanics of thin films under in-plane stress conditions, which are well studied [67]. A particularly striking demonstration of the coupling between in-plane stress and out-off-plane strain during the swelling of substrate-supported polymers can be found in a study of the hydration of thin Nafion films on silicon in Ref. [75]. That study presents a more general form of eqs (8)–(10), applicable to large strain amplitudes, arranged to enable the determination of an unknown biaxial modulus. In the limit of small strains, their results agree with those of the present study. Furthermore, Ref. [75] combines wafer curvature data for the in-plane stress with x-ray reflectivity data for the out-of-plane strain in the same system, confirming the consistency of the description. This finding supports eqs (5)–(7) as a basis for estimating the coupling parameters of thin PPy films, provided that Ω, ν and Y are known with sufficient accuracy.

We now combine eqs (8)–(10) with literature values of Ω, Y and ν and compare the results to the experimental determined coupling parameters. The perchlorate anion has a valency of $z = -1$. Ionic volumes in aqueous solutions are elusive and simply taking ionic radii leads to significant errors [76,77]. Yet, the molar volume of solvated perchlorate anions in water is known from systematic studies exploring solution densities. These techniques indicate $\Omega = 49\ \mathrm{cm^3/mol}$ [76–80]. We adopt this value as a best guess of the partial molar volume of the solvated perchlorate ion in PPy. Equation (8) then suggests $\psi = 0.17\ \mathrm{mm^3/C}$. While experimental data for ψ of the PPy-perchlorate system has not been reported, our estimate is well within the range of results for a variety of other PPy(co-ion) systems and solvents, namely $\psi = 0.03$ to $0.5\ \mathrm{mm^3/C}$ [5,29,35,36].

The above considerations emphasize that the mechanical boundary conditions significantly influence the strain-charge response of the PPy film. Different strain-charge coupling coefficients will be observed, depending on the direction of the measured strain. Quoted values [5,29,35,36] for ψ were obtained from μm-thick films, which were uniaxially loaded by a constant force. Under this condition, the measured strain corresponds to the free expansion as calculated by eq (8). By contrast, Smela and Gadegaard [21] investigated the normal expansion of PPy films clamped on rigid substrates. There, the strain-charge coupling coefficient would be larger, as calculated by eq (9). Yet, the correlation between strain and transferred charge was not explored in Ref. [21], and the value of ψ_z was not reported. If we adopt $\nu = 0.4$ for PPy [25,81], eq (9) yields $\psi_z = 0.39\ \mathrm{mm^3/C}$ for the strain-charge coupling coefficient in normal direction.

Y of PPy depends significantly on the manufacturing conditions, the species of counter ions, the solvent and the oxidation state. Reported values span about one order of magnitude, from 200 to 3600 MPa [9,10,25,35,82,83]. The system used in our work, perchlorate-doped PPy in aqueous solution at electrode potentials of 0.4–0.8 V vs. SHE, has been thoroughly studied and Young's modulus determined as $Y = 500\pm10$ MPa [9]. With this parameter, and with $\Omega = 49\ \mathrm{cm^3/mol}$ as above, eq (10) suggests $\xi = -141$ mV. The agreement with our experimental result, -151 ± 11 mV, is remarkable. The independent estimate of ξ, based on literature data and simple physical models, confirms our experimental findings and emphasizes their validity.

To summarize: In our experimental study we investigated the stress-charge coupling of thin PPy films in aqueous perchloric acid. We deposited nm-thick PPy films on μm-thick silicon cantilevers and cyclically varied their electrode potential. In response to that variation, we recorded the curvature changes of the silicon substrates as well as the transferred charge. The curvature variation is a result of the change in film stress and enables a precise evaluation of the stress-charge coupling parameter. This parameter and the volumetric capacitance are stable over repeated cycles and are independent of the film thickness. Both parameters attain unique values in the potential range under study, consistent with the notion that a single mechanism is active. We obtain an independent estimate of the stress-charge coupling strength by combining a micromechanical analysis of ion insertion into the polymer with published data for the ionic molar volume and the elastic constants of PPy. The two approaches are in excellent agreement.

The stability and linearity of the electro-mechanical response in our study qualifies the results as particularly robust and the independent verification provides further confirmation of our stress-charge coupling coefficient. Our results for the intrinsic materials parameters behind the actuation with PPy may contribute to provide the basis for an informed discussion of the performance of more complex actuator geometries.

Acknowledgments

This work was supported by the German Research Foundation (DFG) via SFB 986 M^3, project B2. We acknowledge Stella Gries and Manuel Brinker (Hamburg University of Technology, SFB 986 M^3, project B7) for the AFM measurements.

Appendix A. Supplementary data

Supplementary data to this article can be found online at https://doi.org/10.1016/j.electacta.2019.05.166.

References

[1] H. Shirakawa, E.J. Louis, A.G. MacDiarmid, C.K. Chiang, A.J. Heeger, Synthesis of electrically conducting organic polymers: halogen derivatives of polyacetylene, $(CH)_x$, J. Chem. Soc., Chem. Commun. 16 (1977) 578–580.
[2] C.K. Chiang, C. Fincher Jr., Y.W. Park, A.J. Heeger, H. Shirakawa, E.J. Louis, S.C. Gau, A.G. MacDiarmid, Electrical conductivity in doped polyacetylene, Phys. Rev. Lett. 39 (1977) 1098.
[3] A.J. Heeger, Semiconducting and metallic polymers: the fourth generation of polymeric materials (Nobel lecture), Angew. Chem. Int. Ed. 40 (2001) 2591–2611.
[4] T.A. Skotheim, J. Reynolds, Handbook of Conducting Polymers, 3rd ed., CRC

Press, Boca Raton, 2007.
[5] J.D. Madden, P.G. Madden, I.W. Hunter, Conducting polymer actuators as engineering materials, Proc. SPIE 4695 (2002) 176–190.
[6] J.L. Bredas, G.B. Street, Polarons, bipolarons, and solitons in conducting polymers, Acc. Chem. Res. 18 (1985) 309–315.
[7] P. Burgmayer, R.W. Murray, An ion gate membrane: electrochemical control of ion permeability through a membrane with an embedded electrode, J. Am. Chem. Soc. 104 (1982) 6139–6140.
[8] P. Burgmayer, R.W. Murray, Ion gate electrodes. Polypyrrole as a switchable ion conductor membrane, J. Phys. Chem. 88 (1984) 2515–2521.
[9] T. Otero, J.L. Cascales, G.V. Arenas, Mechanical characterization of free-standing polypyrrole film, Mater. Sci. Eng. C 27 (2007) 18–22.
[10] T. Shoa, T. Mirfakhrai, J.D. Madden, Electro-stiffening in polypyrrole films: dependence of Young's modulus on oxidation state, load and frequency, Synth. Met. 160 (2010) 1280–1286.
[11] F. Selampinar, L. Toppare, U. Akbulut, T. Yalçin, Ş. Süzer, A conducting composite of polypyrrole II. As a gas sensor, Synth. Met. 68 (1995) 109–116.
[12] W. Takashima, K. Hayasi, K. Kaneto, Force detection with Donnan equilibrium in polypyrrole film, Electrochem. Commun. 9 (2007) 2056–2061.
[13] M.S. Lee, H.S. Kang, H.S. Kang, J. Joo, A.J. Epstein, J.Y. Lee, Flexible all-polymer field effect transistors with optical transparency using electrically conducting polymers, Thin Solid Films 477 (2005) 169–173.
[14] T. Otero, J. Martinez, J. Arias-Pardilla, Biomimetic electrochemistry from conducting polymers. A review: artificial muscles, smart membranes, smart drug delivery and computer/neuron interfaces, Electrochim. Acta 84 (2012) 112–128.
[15] K. Jurewicz, S. Delpeux, V. Bertagna, F. Beguin, E. Frackowiak, Supercapacitors from nanotubes/polypyrrole composites, Chem. Phys. Lett. 347 (2001) 36–40.
[16] J.-H. Sung, S.-J. Kim, K.-H. Lee, Fabrication of microcapacitors using conducting polymer microelectrodes, J. Power Sources 124 (2003) 343–350.
[17] T. Osaka, T. Momma, H. Ito, B. Scrosati, Performances of lithium/gel electrolyte/polypyrrole secondary batteries, J. Power Sources 68 (1997) 392–396.
[18] Q. Pei, O. Inganäs, Electrochemical applications of the bending beam method; a novel way to study ion transport in electroactive polymers, Solid State Ionics 60 (1993) 161–166.
[19] T. Shoa, J.D. Madden, T. Mirfakhrai, G. Alici, G.M. Spinks, G.G. Wallace, Electromechanical coupling in polypyrrole sensors and actuators, Sensors and Actuators . 161 (2010) 127–133.
[20] J.D. Madden, R.A. Cush, T.S. Kanigan, I.W. Hunter, Fast contracting polypyrrole actuators, Synth. Met. 113 (2000) 185–192.
[21] E. Smela, N. Gadegaard, Volume change in polypyrrole studied by atomic force microscopy, J. Phys. Chem. B 105 (2001) 9395–9405.
[22] S. Hara, T. Zama, W. Takashima, K. Kaneto, Free-standing polypyrrole actuators with response rate of 10.8% s^{-1}, Synth. Met. 149 (2005) 199–201.
[23] S. Hara, T. Zama, W. Takashima, K. Kaneto, Tris (trifluoromethylsulfonyl) methide-doped polypyrrole as a conducting polymer actuator with large electrochemical strain, Synth. Met. 156 (2006) 351–355.
[24] R. Baughman, Conducting polymer artificial muscles, Synth. Met. 78 (1996) 339–353.
[25] A. Mazzoldi, A. Della Santa, D. De Rossi, Conducting polymer actuators: properties and modeling, Poly. Sensor Actuator 68 (2000) 207–244. Springer.
[26] A. Hutchison, T. Lewis, S. Moulton, G. Spinks, G. Wallace, Development of polypyrrole-based electromechanical actuators, Synth. Met. 113 (2000) 121–127.
[27] T. Otero, M. Cortes, Artificial muscle: movement and position control, Chem. Commun. 3 (2004) 284–285.
[28] M. Kaneko, M. Fukui, W. Takashima, K. Kaneto, Electrolyte and strain dependences of chemomechanical deformation of polyaniline film, Synth. Met. 84 (1997) 795–796.
[29] J.D. Madden, P.G. Madden, I.W. Hunter, Polypyrrole actuators: modeling and performance, Proc. SPIE 4329 (2001) 72–84.
[30] L. Bay, T. Jacobsen, S. Skaarup, K. West, Mechanism of actuation in conducting polymers: osmotic expansion, J. Phys. Chem. B 105 (2001) 8492–8497.
[31] Q. Pei, O. Inganäs, Electrochemical applications of the bending beam method. 1. Mass transport and volume changes in polypyrrole during redox, J. Phys. Chem. 96 (1992) 10507–10514.
[32] T. Otero, J. Martínez, B. Zaifoglu, Using reactive artificial muscles to determine water exchange during reactions, Smart Mater. Struct. 22 (2013) 104019.
[33] E.D. Daneshvar, E. Smela, Characterization of conjugated polymer actuation under cerebral physiological conditions, Adv. Healthc. Mater. 3 (2014) 1026–1035.
[34] L. Valero, T.F. Otero, J.G. Martínez, Exchanged cations and water during reactions in polypyrrole macroions from artificial muscles, ChemPhysChem 15 (2014) 293–301.
[35] P. Chiarelli, A.D. Santa, D. De Rossi, A. Mazzoldi, Actuation properties of electrochemically driven polypyrrole free-standing films, J. Intell. Mater. Syst. Struct. 6 (1995) 32–37.
[36] P.A. Anquetil, D. Rinderknecht, N.A. Vandesteeg, J.D. Madden, I.W. Hunter, Large strain actuation in polypyrrole actuators, Proc. SPIE 5385 (2004) 380–388.
[37] E. Smela, O. Inganäs, I. Lundström, Controlled folding of micrometer-size structures, Science 268 (1995) 1735–1738.
[38] E. Smela, Conjugated polymer actuators for biomedical applications, Adv. Mater. 15 (2003) 481–494.
[39] C. Plesse, F. Vidal, H. Randriamahazaka, D. Teyssié, C. Chevrot, Synthesis and characterization of conducting interpenetrating polymer networks for new actuators, Polymer 46 (2005) 7771–7778.
[40] G. Alici, N.N. Huynh, Predicting force output of trilayer polymer actuators, Sensors and Actuators A 132 (2006) 616–625.
[41] V. Woehling, G.T. Nguyen, C. Plesse, S. Cantin, J.D. Madden, F. Vidal, Interpenetrating polymer network (IPN) as tool for tuning electromechanical properties of electrochemical actuator operating in open-air, Sensors and Actuators. B Chem. 256 (2018) 294–303.
[42] D. Melling, J.G. Martinez, E.W. Jager, Conjugated polymer actuators and devices: progress and opportunities, Adv. Mater. (2019) 1808210.
[43] J. Weissmüller, D. Kramer, Balance of force at curved solid metal-liquid electrolyte interfaces, Langmuir 21 (2005) 4592–4603.
[44] M. Smetanin, R. Viswanath, D. Kramer, D. Beckmann, T. Koch, L. Kibler, D. Kolb, J. Weissmüller, Surface stress-charge response of a (111)-textured gold electrode under conditions of weak ion adsorption, Langmuir 24 (2008) 8561–8567.
[45] J.M. Albina, C. Elsässer, J. Weissmüller, P. Gumbsch, Y. Umeno, Ab initio investigation of surface stress response to charging of transition and noble metals, Phys. Rev. B 85 (2012) 125118.
[46] Q. Deng, V. Gopal, J. Weissmüller, Less noble or more noble: how strain affects the binding of oxygen on gold, Angew. Chem. 127 (2015) 13173–13177.
[47] A. Michl, J. Weissmüller, S. Müller, Electrocapillary coupling at metal surfaces from first principles: on the impact of excess charge on surface stress and relaxation, Langmuir 34 (2018) 4920–4928.
[48] A. Kivilo, Z. Zondaka, A. Kesküla, P. Rasti, T. Tamm, R. Kiefer, Electro-chemo-mechanical deformation properties of polypyrrole/dodecylbenzenesulfate linear actuators in aqueous and organic electrolyte, RSC Adv. 6 (2016) 96484–96489.
[49] I. Põldsalu, M. Harjo, T. Tamm, M. Uibu, A.-L. Peikolainen, R. Kiefer, Inkjet-printed hybrid conducting polymer-activated carbon aerogel linear actuators driven in an organic electrolyte, Sensors and Actuators A. B Chem. 250 (2017) 44–51.
[50] J. Zhang, L.-B. Kong, B. Wang, Y.-C. Luo, L. Kang, In-situ electrochemical polymerization of multi-walled carbon nanotube/polyaniline composite films for electrochemical supercapacitors, Synth. Met. 159 (2009) 260–266.
[51] T.I. Schnoor, U. Vainio, L.-H. Shao, E.T. Lilleodden, M. Müller, A. Schreyer, K. Schulte, B. Fiedler, Nanostructured mwcnt/polypyrrole actuators with anisotropic strain response, Adv. Eng. Mater. 18 (2016) 597–607.
[52] M. Beregoi, A. Evanghelidis, V.C. Diculescu, H. Iovu, I. Enculescu, Polypyrrole actuator based on electrospun microribbons, ACS Appl. Mater. Interfaces 9 (2017) 38068–38075.
[53] K. Wang, C. Stenner, J. Weissmüller, A nanoporous gold-polypyrrole hybrid nanomaterial for actuation, Sensors and Actuators. B Chem. 248 (2017) 622–629.
[54] K.K. Lee, Y. Dobashi, P.R. Herman, J.D. Madden, V.X. Yang, Improved charging and strain rates by laser perforating polypyrrole actuator electrodes, Smart Mater. Struct. 28 (2018), 015028.
[55] W. Haiss, R.J. Nichols, J.K. Sass, K.P. Charle, Linear correlation between surface stress and surface charge in anion adsorption on Au(111), J. Electroanal. Chem. 452 (1998) 199–202.
[56] W. Haiss, Surface stress of clean and adsorbate-covered solids, Rep. Prog. Phys. 64 (2001) 591–648.
[57] J. Weissmüller, R.N. Viswanath, D. Kramer, P. Zimmer, R. Würschum, H. Gleiter, Charge-induced reversible strain in a metal, Science 300 (2003) 312–315.
[58] H.J. Jin, X.L. Wang, S. Parida, K. Wang, M. Seo, J. Weissmüller, Nanoporous Au-Pt alloys as large strain electrochemical actuators, Nano Lett. 10 (2010) 187–194.
[59] E. Detsi, M.S. Sellès, P.R. Onck, J.T.M. De Hosson, Nanoporous silver as electrochemical actuator, Scripta Mater. 69 (2013) 195–198.
[60] T.F. Otero, J.G. Martinez, Activation energy for polypyrrole oxidation: film thickness influence, J. Solid State Electrochem. 15 (2011) 1169–1178.
[61] A.F. Diaz, J.I. Castillo, J. Logan, W.-Y. Lee, Electrochemistry of conducting polypyrrole films, J. Electroanal. Chem. Interfacial Electrochem. 129 (1981) 115–132.
[62] S.J. Hahn, W.E. Stanchina, W.J. Gajda, P. Vogelhut, The effect of growth rate variation on the conductivity and morphology of polypyrrole thin films, J. Electron. Mater. 15 (1986) 145–149.
[63] E. Chason, Resolution and Sensitivity of Stress Measurements with the K-Space Multi-Beam Optical Sensor (MOS) System, Sandia National Laboratories, San Antonio, TX, USA, 2005.
[64] Q. Van Overmeere, J.-F. Vanhumbeeck, J. Proost, On the use of a multiple beam optical sensor for in situ curvature monitoring in liquids, Rev. Sci. Instrum. 81 (2010), 045106.
[65] G. Abadias, E. Chason, J. Keckes, M. Sebastiani, G.B. Thompson, E. Barthel, G.L. Doll, C.E. Murray, C.H. Stoessel, L. Martinu, Stress in thin films and coatings: current status, challenges, and prospects, J. Vac. Sci. Technol.: Vacuum, Surfaces, and Films 36 (2018), 020801.
[66] G.G. Stoney, The tension of metallic films deposited by electrolysis, Proc. Roy. Soc. Lond. A 82 (1909) 172–175.
[67] W.D. Nix, Mechanical properties of thin films, Metallurgical transactions A 20 (1989) 2217.
[68] M.A. Hopcroft, W.D. Nix, T.W. Kenny, What is the Young's modulus of silicon? Journal of microelectromechanical systems 19 (2010) 229–238.
[69] T. Lewis, G. Wallace, C. Kim, D. Kim, Studies of the overoxidation of

polypyrrole, Synth. Met. 84 (1997) 403–404.
[70] Y. Li, On the large overpotential of the first reduction of polypyrrole perchlorate films in organic solutions, Electrochim. Acta 42 (1997) 203–210.
[71] C. Song, J. Zhang, PEM Fuel Cell Electrocatalysts and Catalyst Layers: Fundamentals and Applications, Springer, 2008, pp. 89–134.
[72] D. Melling, S. Wilson, E.W. Jager, The effect of film thickness on polypyrrole actuation assessed using novel non-contact strain measurements, Smart Mater. Struct. 22 (2013) 104021.
[73] A.J. Bard, L.R. Faulkner, Electrochemical methods: fundamentals and applications, 2nd ed., John Wiley & Sons, Inc., New York, 2001.
[74] M.C. Lafouresse, U. Bertocci, C.R. Beauchamp, G.R. Stafford, Simultaneous electrochemical and mechanical impedance spectroscopy using cantilever curvature, J. Electrochem. Soc. 159 (2012) H816–H822.
[75] K.A. Page, J.W. Shin, S.A. Eastman, B.W. Rowe, S. Kim, A. Kusoglu, K.G. Yager, G.R. Stafford, In situ method for measuring the mechanical properties of Nafion thin films during hydration cycles, ACS Appl. Mater. Interfaces 7 (2015) 17874–17883.
[76] J. Akitt, Limiting single-ion molar volumes. Intrinsic volume as a function of the solvent parameters, J. Chem. Soc., Faraday Trans. 1: Physical Chemistry in Condensed Phases 76 (1980) 2259–2284.
[77] Y. Marcus, Electrostriction in electrolyte solutions, Chem. Rev. 111 (2011) 2761–2783.
[78] F.J. Millero, Molal volumes of electrolytes, Chem. Rev. 71 (1971) 147–176.
[79] B. Conway, E. Ayranci, Effective ionic radii and hydration volumes for evaluation of solution properties and ionic adsorption, J. Solut. Chem. 28 (1999) 163–192.
[80] Y. Marcus, G. Hefter, Standard partial molar volumes of electrolytes and ions in nonaqueous solvents, Chem. Rev. 104 (2004) 3405–3452.
[81] Y. Wu, G. Alici, J.D. Madden, G.M. Spinks, G.G. Wallace, Soft mechanical sensors through reverse actuation in polypyrrole, Adv. Funct. Mater. 17 (2007) 3216–3222.
[82] P. Murray, G. Spinks, G. Wallace, R. Burford, Electrochemical induced ductile–brittle transition in tosylate-doped (pTS) polypyrrole, Synth. Met. 97 (1998) 117–121.
[83] J.D. Madden, R.A. Cush, T.S. Kanigan, C.J. Brenan, I.W. Hunter, Encapsulated polypyrrole actuators, Synth. Met. 105 (1999) 61–64.